PROTEINS: Structure, Function, and Genetics 53:656–666 (2003)

Accessibility of Oxygen With Respect to the Heme Pocket in Horseradish Peroxidase

Mazdak Khajehpour,* Ivo Rietveld, Sergei Vinogradov, Ninad V. Prabhu, Kim A. Sharp, and Jane M. Vanderkooi
Department of Biochemistry and Biophysics, School of Medicine, University of Pennsylvania, Philadelphia, Pennsylvania

ABSTRACT **Oxygen and other molecules of similar size take part in a variety of protein reactions. Therefore, it is critical to understand how these small molecules penetrate the protein matrix. The protein system studied in this case is horseradish peroxidase (HRP). We have converted the native HRP into a phosphorescent analog by replacing the heme prosthetic group by Pd-mesoporphyrin. Oxygen readily quenches the phosphorescence of Pd porphyrins, and this can be used to characterize oxygen diffusion through the protein matrix. Our measurements indicate that solvent viscosity and pH modulate the accessibility of the heme pocket relative to small molecules. The binding of the substrate benzohydroxamic acid (BHA) to the protein drastically impedes oxygen access to the heme pocket. These results indicate that, first, the penetration of small molecules through the protein matrix is a function of protein dynamics, and second, there are specific pathways for the diffusion of these molecules. The effect of substrate and pH on protein dynamics has been investigated with the use of molecular dynamics calculations. We demonstrate that the model of a "fluctuating entry point," as suggested by Zwanzig (J Chem Phys 1992;97:3587–3589), properly describes the diffusion of oxygen through the protein matrix. Proteins 2003;53:656–666.**

Key words: protein dynamics; phosphorescence quenching; porphyrin

INTRODUCTION

Many protein reactions involve the diffusion of a small molecule from the bulk solution to an active site inside the protein. The penetration of these small molecules in proteins is a function of protein dynamics. A classic case in point is that of myoglobin; Perutz has pointed out that the crystal structure of the protein is too compact to accommodate oxygen penetration. Therefore, it is the dynamic motion of the protein that allows the oxygen to access the active site of myoglobin.[1] The importance of the role of protein dynamics on the movement of small molecules has been studied by a variety of techniques. For example, the Frauenfelder, Eaton, and Friedman groups have studied the photodissociation and rebinding of CO and O_2 ligands from the iron in heme proteins and verified the role of protein dynamics on the motion of these ligands in the heme pocket.[2–12] Other examples involving similar-size species in ligand/substrate/reactant systems include superoxide in the superoxide dismutase enzymatic system,[13] and hydrogen peroxide in catalase.[14]

The quenching of emission is an alternative method to monitor the motion of species in proteins. The pioneering work of Weber and associates heralded the application of the quenching of tryptophan fluorescence to the investigation of protein dynamics and its role in facilitating the diffusion of small molecules inside the protein matrix.[15–17] Tryptophan fluorescence provides a powerful tool for investigating protein dynamics; however, it is hampered by the short lifetime of the excited singlet state compared to the time scale of long-range protein dynamic motions. This leads to multiexponential fluorescence decay curves that complicate quantification of protein dynamic effects. In contrast to fluorescence, room temperature phosphorescence occurs in the time scale of many long-range protein motions. Reviews by Vanderkooi[18] and Subramanian et al. [19] illustrate the versatility of room-temperature tryptophan phosphorescence in monitoring protein dynamics and flexibility. The penetration of different phosphorescent quenchers in protein matrices has been studied by Calhoun et al.,[20] and protein dynamics have been studied by either monitoring the quenching of tryptophan phosphorescence by oxygen and acrylamide as a function of temperature and solvent viscosity,[21,22] or measuring the time-dependent change in the tryptophan phosphorescence lifetime as a function of the deuterium exchange.[23–25]

One of the most versatile and, at the same time, most biologically relevant quenchers of luminescence is molecular oxygen. Oxygen is an ideal probe of protein dynamics because, first, it is a nonpolar molecule and, therefore, would not interact strongly with any of the residues in the protein; second, it is a small molecule that can penetrate the protein matrix easier than most; third, it is a nonspecific quencher of photochemically excited molecules; and finally, it takes part in many protein reactions, which

Abbreviations: HRP, horseradish peroxidase; MPHRP, mesoporphyrin-IX–substituted horseradish peroxidase; Pd-MPHRP, palladium-bound mesoporphyrin-IX–substituted horseradish peroxidase; BHA, benzohydroxamic acid

Grant sponsor: National Institute of Health; Grant number: PO1 48130.

*Correspondence to: Mazdak Khajehpour, Department of Biochemistry and Biophysics, School of Medicine, University of Pennsylvania, Philadelphia, PA 19104. E-mail: mazdak@mail.med.upenn.edu

Received 17 December 2002; Accepted 6 February 2003

makes the specific study of oxygen diffusion in the protein biologically significant. Understanding the diffusion of oxygen in proteins is extremely important in heme proteins. The reactions of these proteins involve either oxygen or hydrogen peroxide. These molecules are approximately the same size. Therefore, conditions that modulate oxygen penetration also affect the diffusion of hydrogen peroxide within the protein.

Since the work of Weber, a large body of research involving the motion of quenchers in proteins has been accomplished.[20,26–31] These studies indicate that the motion of quenchers in proteins is "gated" (i.e., the passing of quenchers depends on the protein making a sufficient conformational change, enabling the quencher to pass through). The question that remains is whether the protein matrix is homogeneously penetrable by small molecules, or whether these molecules access the interior of the proteins through specific pathways.

We have endeavored to answer this question by employing the heme-containing enzyme horseradish peroxidase (HRP). Like many heme proteins involved in synthetic reactions, including enzymes such as cytochrome P450 and peroxidases, the first reaction of HRP requires the penetration of a small molecule, with the formation of an activated enzyme species. The sequence of reactions for HRP is known.[32–34] The first step is the binding of H_2O_2:

$$Fe^{3+}\ HRP + H_2O_2 \rightarrow$$

$$\text{Compound I (HRPFeO + porphyrin cation)} + H_2O.$$

The enzyme, as Compound I, then reacts with a wide range of aromatic substances, leading to oxidation and the formation of a free-radical compound. The diffusion of hydrogen peroxide toward the heme prosthetic group is a crucial step for enzyme activity. HRP binds tightly to the competitive inhibitor benzohydroxamic acid (BHA).[35–42] Substrate binding causes the protein to become more rigid in the near vicinity of the binding site. If oxygen can only access the heme pocket via specific channels, the binding of BHA to the protein might have a much more drastic effect on the diffusion of oxygen toward the heme than what may be expected from its size.

In this work, we investigate the mechanism of oxygen and hydrogen peroxide diffusion from the bulk solution to the heme prosthetic group. To this end, we substitute the nonemitting heme prosthetic group with a phosphorescent palladium mesoporphyrin (Pd-MP).[43–45] The phosphorescence of Pd-MP is readily quenched by molecular oxygen. Therefore, the quenching of the phosphorescence of Pd-MP inside horseradish peroxidase (Pd-MPHRP) characterizes the diffusion of oxygen toward the heme.

The diffusion of oxygen toward the heme prosthetic group involves two steps: First, oxygen has to diffuse from the bulk solution toward the protein surface; second, it needs to penetrate the protein matrix. To separate these two contributions, we have employed as a reference compound a water-soluble generation 3 polyglutamic Pd-porphyrin dendrimer (PdPorphGlu^{3}OH).[46] This dendritic porphyrin has a phosphorescent core similar to Pd-MP; in aqueous solution, it has a relatively open conformation. The quenching rate of the porphyrin dendrimer phosphorescence represents the diffusion of oxygen in the bulk solution.

We have investigated the effect of temperature, solvent viscosity, and substrate on the diffusion of oxygen through the protein matrix. Our experimental results indicate that oxygen and other small molecules access the heme pocket via a channel, and that the diffusion of these molecules can be well described by the bottleneck model developed by Zwanzig.[47] We have also employed 6-bromo-2-naphthyl sulfate (BNS) as an external phosphorescent probe of heme accessibility. Schuh and collaborators introduced the use of this molecule.[48–50] BNS is about the same size as the aromatic substrates of HRP and can be used to determine whether larger molecules can access the heme pocket. We have also performed molecular dynamics (MD) simulations to investigate the effect of substrate binding on the motion of the residues that form the access channel. The binding of BHA influences the motion of these residues. From these results, we draw conclusions about the mechanism of the diffusion of small molecules from the bulk solution to the heme pocket.

MATERIALS AND METHODS

Materials

Water was deionized and then glass-distilled. HRP type C (HRPC), glucose, glucose oxidase, and catalase were obtained from Sigma Chemical Company (St. Louis, MO). Aldrich Chemical Company (Milwaukee, WI) supplied BHA. HRP was purified as described,[51] based on Paul's procedure.[52] Pd-mesoporphyrin IX was obtained from Porphyrin Products (Logan, UT) and incorporated into HRP to form Pd-MP-HRP, as was done previously.[53] PdPorphGlu^{3}OH was synthesized and purified according to Vinogradov et al.[46] The molecular weight (MW) of Pd porphGlu^{3}OH in polycarboxylic acid form is 4510.

Instrumentation

Steady-state emission spectra were obtained with a Fluorolog-3 Spex instrument equipped with a 928 Hammamatsu photomultiplier tube. When phosphorescence spectra were obtained, a Spex 19340 phosphorimeter module coupled to the Fluorolog-3 instrument was used. All spectra were corrected for lamp fluctuations. We analyzed the results with commercially available software, Sigmaplot (Chicago, IL). The samples were deoxygenated via a coupled enzyme reaction, as described previously.[20]

We determined phosphorescence lifetimes as a function of oxygen-concentration titrations using an in-house constructed system.[54] Two main components of the system are a frequency domain phosphorometer (Oxygen Enterprises, Ltd.)[55] and a sensitive, Clark-type oxygen electrode (C.J. Koch, Canadian Patent 30 June 1992, 1304449). The special design of the electrode causes its zero current to be in the order of a few *p*A, whereas the noise at this level is only about 4% of the signal, permitting accurate O_2 measurements at O_2 partial pressures of less than 0.05

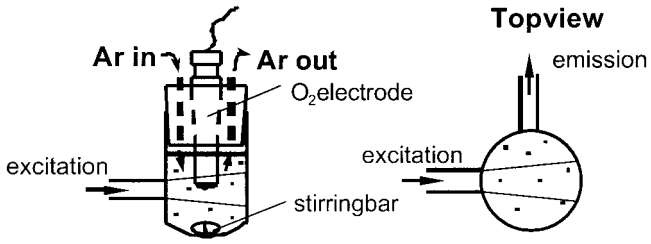

Fig. 1. Phosphorescence lifetime/oxygen concentration titration setup.

mmHg. The phosphorometer allows for complete, in-phase correction of the signal in the phase-locked mode. A cylindrical cuvette (Fig. 1) was placed in a thermostatic jacket with electronic temperature control (0.1°C precision), set on the top of a magnetic stirrer. The excitation light and emitted phosphorescence were carried to and from the sample by 3 mm/ID light guides. The sample solution was placed in a cuvette and sealed by a stopper with inserted electrode and two ports for Ar inlet and outlet. Ar was passed over the surface of continuously stirred solution, gradually replacing air, while the output of the electrode amplifier and the phosphorescence lifetime readings were synchronously recorded into a file every 10 s.

At least three data sets were independently acquired for each compound and set of conditions, providing adequate experimental statistics (raw titration data are available upon request).

Computational Methods

Molecular Dynamics

The force field for the MD simulations of HRPC was the CHARMM 22 all-atom parameter set,[56] and simulations were run with the CHARMM 27 program suite.[57] Modeling a system the size of HRPC in a box of explicit solvent with periodic boundary conditions is computationally demanding (the total system size would be greater than 40,000 atoms). Hence, the solvent was modeled as a continuum by incorporating the solvent contribution to the free energy and forces from a high-speed Poisson–Boltzmann solver,[58] implemented as the ZAP C++ toolkit (OpenEye Software, Santa Fe, NM). The ZAP toolkit was interfaced with the CHARMM MD code. For the continuum solvent model, a dielectric of 80 was used. We obtained the apolar contribution to energies and forces from solvent using the solvent-accessible surface area model, with a hydrophobic coefficient of 6 cal/mole/Å^2. Surface areas and derivatives are also obtained from ZAP. Continuum solvent forces were updated every 10 fs. All alpha carbons and the two Ca^{2+} ions were restrained by a force of 24 kcal/mol/A^2 to ensure the overall stability of the protein structure during the course of the simulations, and all bond lengths were constrained by SHAKE. Positional constraints, however, were not applied to any of the heme and BHA atoms, because their relative and translational motions may be of interest. Comparison of this protocol (with ZAP and similar constraints) and an explicit water MD simulation of a smaller protein: calmodulin (with constraints), will be published elsewhere (N.V. Prabhu, K.A. Sharp, personal communication, January 2003).

The starting structure of the simulations of HRPC with BHA is 2ATJ, and those without BHA are 1ATJ.[39,59] We have examined the dynamics at the pore region of five simulations. The crystal structure of Pd-MPHRP is unknown, but of all the available structures, we consider that in which the heme iron is ligated to carbon monoxide to be the structure that most closely resembles Pd-MPHRP, because Pd only coordinates to the porphyrin nitrogen atoms and cannot coordinate to the nearby histidine residue (CO-ligated HRP similarly has no distal histidine coordinated to the central iron atom). The histidines are in the protonated form in these simulations.

The five simulations include the calcium ions from the X-ray structure. Of these, two simulations are of HRPC with and without BHA, and with protonated histidines, to represent the low pH environment. For the two simulations corresponding to the high pH case, the histidines are unprotonated.

Finally, a simulation in which the positively charged Arg38 mutated to the neutral leucine was performed with the non-BHA 1ATJ structure. This final simulation represents the possible case in which the Arg38 may get deprotonated at very high pH. Because BHA does not bind in such an environment (pH $>$ 11), the high pH neutral Arg 38 with BHA simulation was not necessary.

Because the molecular mechanics force field parameters for BHA are not available in the CHARMM 22 set, we have calculated BHA atomic charge and dihedral angles for the simulation parameters as described elsewhere (A. Kaposi, personal communication, February 2003). All simulations were run for 500 ps. All structures were first minimized and, after short heating and equilibration for 50 ps, run with a timestep of 2 fs, for a total duration of 500 ps. Coordinates from every 0.1 ps were used for analysis.

DATA ANALYSIS

Figure 2 depicts the photochemical relaxation mechanism of the porphyrin moiety in the HRP derivatives. If the formation of the triplet state is much more rapid than the decay, the lifetime of the triplet state τ is defined as

$$\tau = \frac{1}{k_e + k_m + k_p + k_q[Q]},$$

in which $[Q]$ is concentration of quencher and all other quantities are defined as in Figure 2. If the inverse of the triplet state lifetime is plotted as a function of the quencher concentration, a Stern–Volmer plot is obtained:

$$\tau^{-1} = k_e + k_m + k_p + k_q[Q] \quad (1)$$

If the inherent bimolecular quenching rate is much faster than the approach of the quencher and phosphor, the measured bimolecular quenching constant is a function of the approach of the two moieties to one another. In this case, the motion of the quencher is a case of diffusion through a heterogeneous medium. We then analyze our

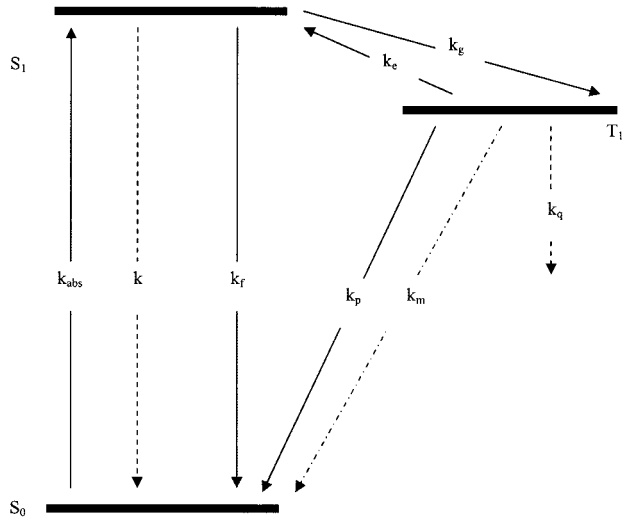

Fig. 2. The energy diagram of the photochemical decay of the singlet and triplet excited states of Pd-MPHRP. In this figure, k_{abs} is the rate for the absorbance, k is the nonradiative decay rate for the excited singlet state, k_f is the rate of fluorescence decay, k_g is the S_1 to T_1 intersystem crossing rate, k_p is the rate of phosphorescence decay, k_e is the T_1 to S_1 intersystem crossing rate, k_m is the nonradiative intersystem crossing rate between T_1 and S_0, and k_q is the quenching rate.

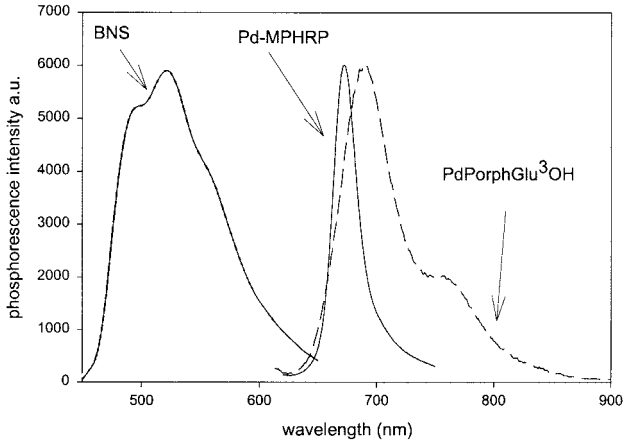

Fig. 3. Phosphorescence emission spectra. BNS: about 30 μM in deoxygenated 50 mM Na acetate, pH 5. Spectra were collected after a 100 μs delay, using λ_{ex} = 275 nm, 7 and 7 nm band-pass for excitation and emission, respectively. Pd-MPHRP: Protein concentration was 25 μM in deoxygenated 50 mM Na acetate, pH 5. The spectrum was recorded in the steady-state mode using λ_{ex} = 396 nm and 1 nm band-pass for both the excitation and emission monochromators. PdPorphGlu^{3}OH: The compound was about 5 μM in deoxygenated water. The spectrum was recorded in the steady-state mode, using λ_{ex} = 524 nm and 2 nm band-pass for both the excitation and emission monochromators.

results via the methodology of Barboy and Feitelson.[31] In this case the process is

$$P_P^* + Q_S \underset{k_{-d}}{\overset{k_d}{\rightleftharpoons}} (P_P^* + Q)_P \overset{k_1}{\rightarrow} (P^*Q)_P \overset{\kappa}{\rightarrow} P_P + Q,$$

where the subscripts P and S indicate the protein and the solvent phases, respectively. The quenching of the porphyrin phosphorescence involves the following steps: Initially, the quencher and the protein encounter each other, represented by k_d. If the phosphor is embedded in the protein, the quencher has to diffuse through the protein matrix, represented by k_1, and κ represents the instantaneous quenching rate once the encounter complex is formed inside the protein. Considering this scheme, and applying the approximations invoked by Barboy and Fietelson,[31] the observed quenching rate constants obtained from the Stern–Volmer equation are, for the protein,

$$k_q(\text{protein}) = 4\pi D_P a, \quad (2)$$

whereas for a free porphyrin,

$$k_q(\text{porphyrin}) = 4\pi D_S a, \quad (3)$$

where D_P and D_S are the diffusion constants of the quencher inside the protein and in solution, and a is the distance of the closest approach.

EXPERIMENTAL RESULTS

Phosphorescence Spectra

The phosphorescence spectra of the three probes used in this study are shown in Figure 3. BNS emits in the range of 450–600 nm. Pd-MPHRP has its emission maximum at 675 nm. The Pd-porphyrin dendrimer PdPorphGlu^{3}OH emits at 690 nm. Its emission is somewhat broader than that of Pd-MPHRP.

Phosphorescence Quenching by Oxygen

In Figure 4, the Stern–Volmer quenching curves of the phosphorescence lifetimes of Pd-MPHRP and the model dendritic compound have been given as a function of oxygen concentration. The oxygen concentration has been determined by standardization of the electrode response to existing solubility data.[60,61] Samples included Pd-MPHRP at pH 5, BHA-Pd-MPHRP complex at the same pH, Pd-MPHRP at high pH, and PdPorphGlu^{3}OH at pH 5. The experiments were carried out at 5, 15, and 25°C. The plotted data are linear, indicating a simple bimolecular quenching process and the absence of complex formation. All samples, except BHA-Pd-MPHRP, show phosphorescence lifetimes in the absence of O_2 that are approximately independent of temperature. For BHA-Pd-MRPHRP, the phosphorescence lifetimes in the absence of O_2 are temperature-dependent, because BHA quenches the Pd-MPHRP phosphorescence via a temperature-dependent mechanism.[62] This reaction does not affect the analysis of quenching, because the O_2 quenching constants are obtained from the slope of the line.

The quenching constants are given in Table I. The dendrimer demonstrates the highest accessibility with respect to O_2, with quenching rate constants ranging from 2.0e9 to 1.1e9 M^{-1} s^{-1}. The quenching constant is consistent with published data on polyglutamic Pd-porphyrin dendrimers and reflects the fact that dendritic polyglutamic branches have an open, sparse conformation in aqueous solutions.[46] In contrast, diffusion through the protein matrix in HRP is much more difficult. The values

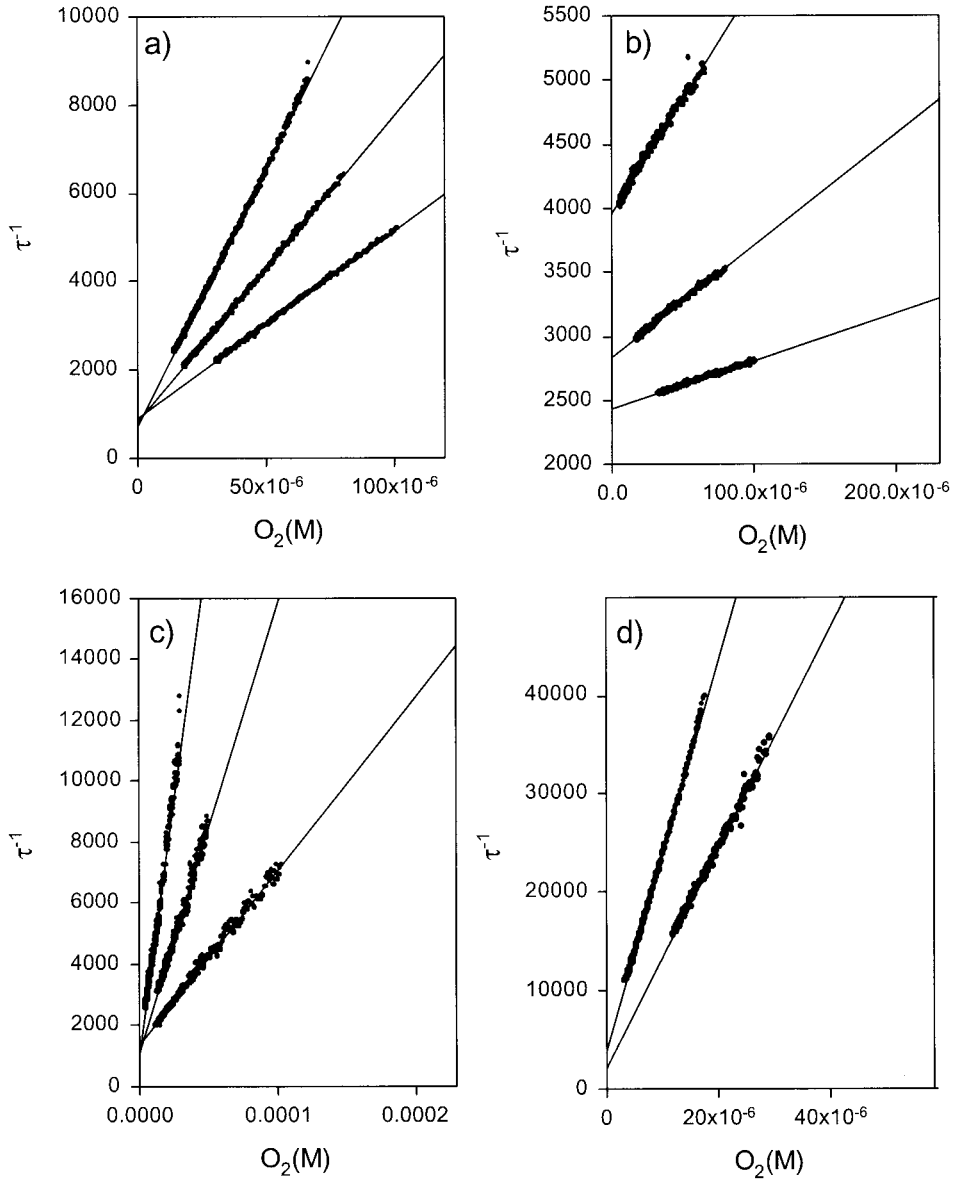

Fig. 4. Observed phosphorescence decay rates, τ^{-1}, as a function of O_2 concentration. The decay rates in each section have been measured at three different temperatures: 25, 15, and 5°C. (**a**) 50 μM Pd-MPHRP in 50 mM Na acetate, pH 5. (**b**) 50 μM Pd-MPHRP and 500 μM BHA in 50 mM Na acetate, pH 5. (**c**) 50 μM Pd-MPHRP in 50 mM Na acetate, pH 10. (**d**) 5 μM Pd-PorphGlu^{3}OH in 50 mM Na acetate, pH 5.

TABLE I. Oxygen Quenching Rate Constants of Pd-MPHRP and Generation-3 Pd Porphyrin Dendrimer at Different Temperatures and Solvent Conditions

Temperature	Quenching rate constant Pd-MPHRP pH = 5	Quenching rate constant Pd-MPHRP pH = 5 with BHA	Quenching rate constant Pd-MPHRP pH = 10	Quenching rate constant Pd-dendrimer pH = 5
25	1.16e8	1.78e7	3.35e8	1.99e9
15	6.92e7	8.73e6	1.47e8	1.40e9
5	4.23e7	3.74e6	5.70e7	1.10e9

range from 1.2e8 to 4.2e7 M^{-1} s^{-1}. For the protein at pH 10, the quenching constants are somewhat higher than for pH 5. This is especially seen at high temperatures, where the fact that the protein becomes more permeable to oxygen may indicate that it becomes less stable at high pH. The effect of BHA on the O_2 quenching is startling. The addition of BHA reduces the quenching constant by a factor of about 6. The energy of activation for O_2 quenching of Pd-MPHRP in the absence of BHA was 8.3 kcal/mol at pH 5 and 14.6 kcal/mol at pH 10. For BHA-Pd-MPHRP,

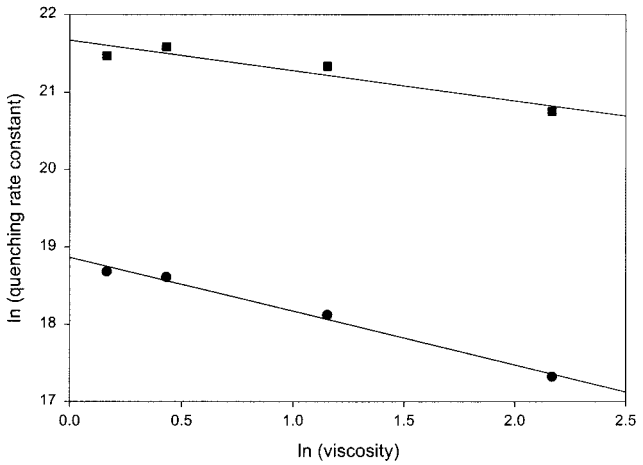

Fig. 5. The oxygen quenching rate constant of excited triplet state Pd-MPHRP (circles) and generation-3 Pd glutamate porphyrin dendrimer (squares) as a function of solvent viscosity.

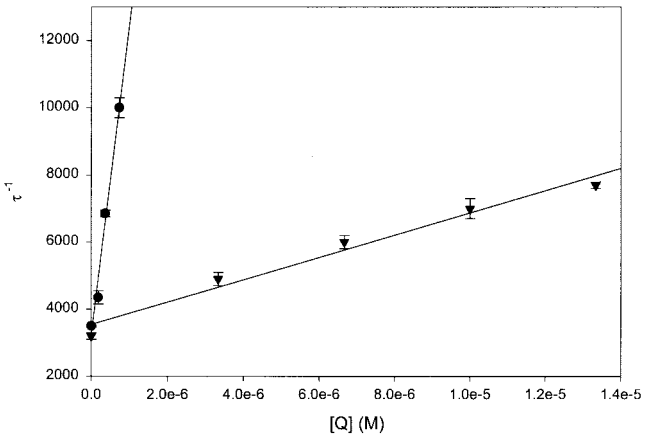

Fig. 6. Phosphorescence quenching curves of BNS as a function of quencher concentration [Q]. The symbols are circles (generation-3 Pd glutamate porphyrin dendrimer) and triangles (horseradish peroxidase). The quenching rate constants are 9.24e9 for dendrimer and 5.0e8 for HRP.

this value was 12.9 kcal/mol at pH 5.0. For comparison, the quenching of the dendrimer phosphorescence had an activation energy of 4.5 kcal/mol, which is consistent with a low diffusion barrier.

Dependence on Solvent Viscosity

In Figure 5 the oxygen quenching rate constant is plotted as a function of solvent viscosity on a log plot. The viscosity was varied by the addition of different amounts of glycerol to the aqueous solution, and all solutions were buffered at pH 5. If the diffusion followed the classic Stokes relationship, the slope of this plot would be -1. However, the slopes are significantly less than that. The values are (-0.7) for the protein and (-0.4) for the dentrimer. A deviation from the Stokes relationship is often seen for O_2 diffusion and is attributed to the fact that O_2 is smaller than the molecules through which it diffuses.

Phosphorescence of BNS

In the above experiments, we compare O_2 quenching for porphyrin in the protein with the model compound PdPorphGlu^{3}OH. Based on the structure, the porphyrin in the model compound should be accessible to the solvent. To test this, the phosphorescence of BNS was examined. In this experiment, BNS is excited and quenching by the porphyrin compound is examined. This reaction can indicate the exposure of heme to solvent,[48] because only when the heme is exposed can it quench the BNS phosphorescence. Phosphorescence quenching profiles of BNS as a function of porphyrin-containing substances are given in Figure 6. The quenching constant was 9.2e9 M^{-1} s^{-1}, much higher than that for native HRP at 4.6e8 M^{-1} s^{-1}.[49] The values for metal-substituted proteins were also measured. The effect of metal substitution on the quenching of BNS is not greater than a factor of 2.

COMPUTATION RESULTS

Dynamics of the Pore Region

The structure of the pore region is shown in Figure 7. Without BHA [Fig. 7(a)], the pore is open to the solvent, indicated by the fact that the heme, shown in dark-blue, is visible. With BHA [Fig. 7(b)], the amino acids (particularly Phe68, shown in green) around the pore are blocking the access to the heme, and only the light-blue of BHA is seen.

Binding of BHA causes the residues in the pore region to become more rigid and also causes a change in the position of some of the residues.[39,59] The dynamics of two residues on opposite sides of the pore, as monitored by the distance from each other, are shown in Figure 8. Without BHA, the distance between Phe68 and Phe142 increases to an average value of ~12 Å from a starting value of ~10 Å. In the presence of BHA, the distance is much closer, about 6.5 Å, and the excursion of the fluctuations reduces to ~0.5 Å.

Examination of the RMS deviations of individual residues in and around the pore region reveal large fluctuations in positions of residues Phe68, Phe142, and Arg178 (Table II). In the simulations BHA, the average root-mean-square deviations (RMSDs) often exceed 2.0 Å. The large RMSDs indicate conformational transitions by these residues. The motions of these amino acids are the most likely ones to modulate the access of molecules to the protein interior. In the simulations with BHA, only Arg178 in the low pH case shows distinct conformational rearrangements.

We also observed that in the absence of BHA, conformational fluctuations of the two phenylalanine residues depended on the charge and pH (Table II). At acidic pH, a low average RMSD of 0.7 Å was observed. As the pH was increased, the deviations increased to 2.5 and 3.4 Å, which showed increasing conformational changes at high and very high pHs, respectively. Comparison of the dihedral angles of Phe68 at low and high pH with the X-ray structure revealed that a transition in the main-chain psi dihedral angle from alpha-helical to the beta region and also transitions in the average values of chi1 and chi2 are responsible for the conformational change (Table III).

These conformational transitions at high pH causes the Phe68 to move from its X-ray–like structure, where it occupies a position above the region between Phe142

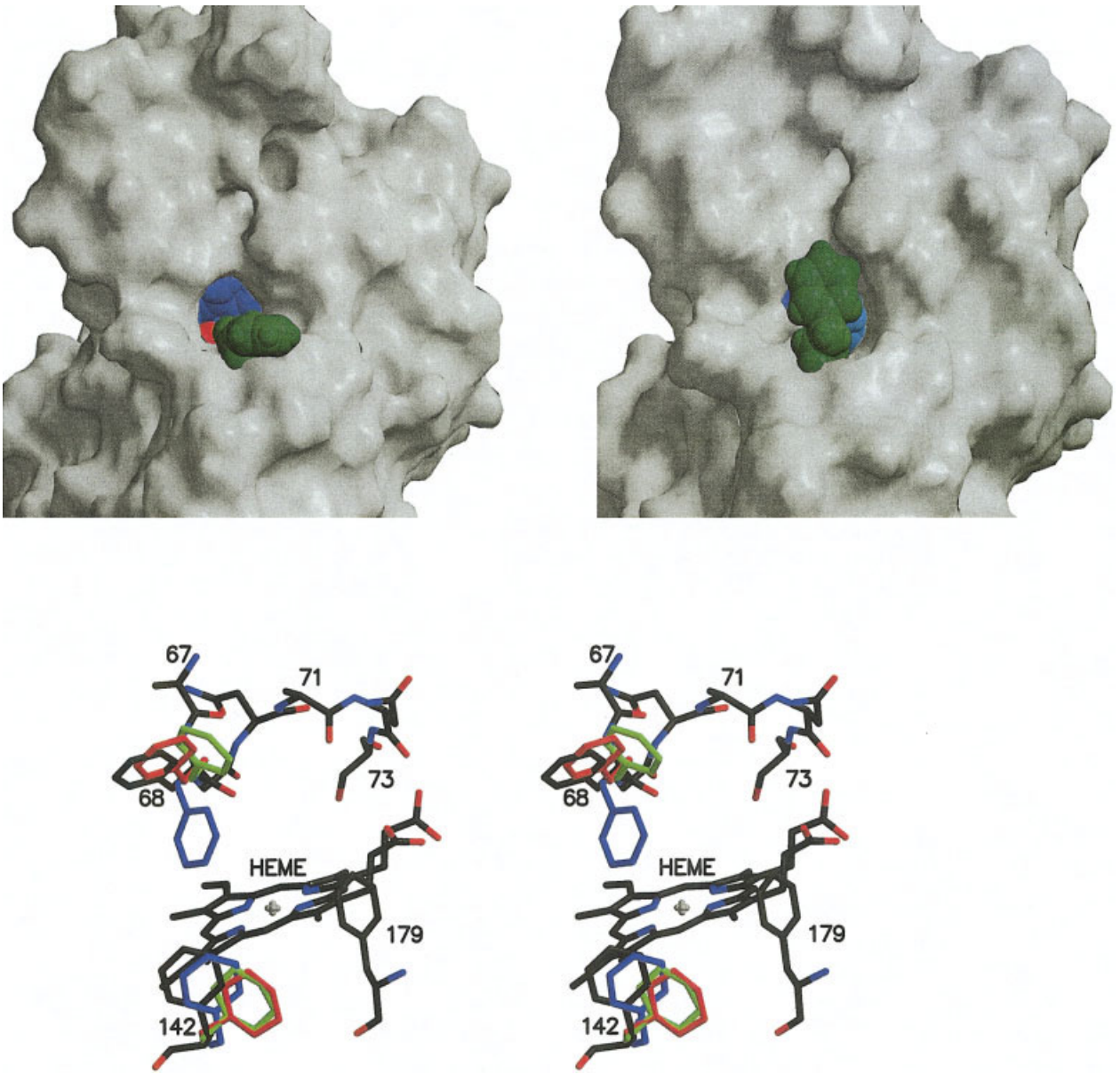

Fig. 7. Top section: structure of the pore region without BHA (top left) and with BHA (top right). Dark-blue, heme; green, Phe68; red, Arg38; light-blue, BHA. Coordinates were taken from 1ATJ for **A** and 2ATJ for **B.** The molecular surface was created with GRASP. Rendering of the figures was done with Molscript and Raster3D. Bottom section: stereograph of the positions of Phe68 and Phe142 obtained during the simulations without BHA. Average: structures of Phe68 and Phe142 are superimposed on selected amino acids from the pore region of HRP without BHA taken from PBD 1ATJ (black). Color Guide: red: simulation 3 (low pH); green: simulation 5 (high pH); blue: simulation 7 (very high pH).

and Phe143, to a position between Phe142 and Phe179 (Fig. 7). The average distances between the centers of Phe68 and Phe142 is around 11 Å for both the low and high pH cases, indicating that the pore remains open. When the low and high pH simulations are compared, the average distance between the center of the Phe68 phenyl ring to the center of the Phe143 ring increases from 11.3 to 12.3 Å, whereas the distance between Phe68 and Phe179 decreases from 12.4 to 11.5 Å. The difference in these values is small, but clearer differences in the orientation of Phe68 relative to the pore can be observed in Figure 7.

In the case in which the positively charged Arg38 was replaced by leucine, the large average RMSD of 3.4 Å was due to Phe68 adopting a conformation in which it blocked the pore above the region between Phe142 and Phe143 (Fig. 7). The average distance of the center of the Phe68 phenyl ring from that of Phe143 is less than 7 Å, similar to the cases in which BHA is present.

The backbone phi and psi dihedral angles for Phe142 are close to X-ray structure values in all the cases. However, in the low and high pH molecular dynamics simulations, the chi1 and chi2 values change from the X-ray values, causing the phenyl ring to get closer to Phe179 and be oriented

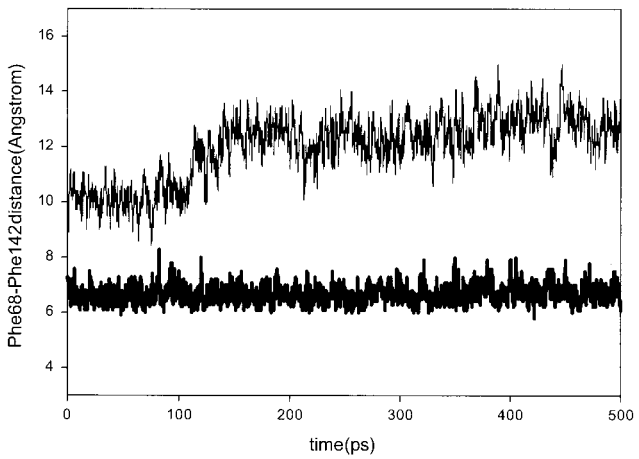

Fig. 8. Distances for center-to-center distance of the aromatic rings of Phe68 and Phe142 are plotted as a function of time. Thin line: without BHA; thick line, with BHA.

TABLE II. Average RMSDs From MD Simulations: Averages Calculated from the Structures in the MD Trajectories

Simulation	phe68	phe142	Arg178
No BHA			
CO/His$^+$	0.7	2.6	2.0
CO/His	2.5	2.2	0.7
CO/His/Leu38	3.4	0.6	1.0
With BHA			
CO/His$^+$	0.5	0.5	2.0
CO/His	1.1	0.7	0.8

parallel to the plane of the heme. At very high pH, the Phe142 prefers an orientation that is close to the X-ray structure, in which the phenyl ring is perpendicular to the plane of the interior heme.

Arg178 also maintains average main-chain dihedral angles close to the X-ray structures for both the low and high pH simulations, as does chi1. The angles chi2, chi3, and chi4 show wider population distributions than the other dihedral angles and, in some cases, multiple transitions between conformational states are observed. The displacement of the Arg178 sidechain is seen in the low pH case in simulations both with and without BHA. Because oxygen entry is high in the non-BHA case and low in the with-BHA case, the conformational mobility of Arg179 is likely to be uncorrelated to oxygen entry; thus, the region near Arg179 is an improbable entry point.

DISCUSSION

As we pointed out in the introduction, understanding the mechanism by which small molecules penetrate proteins and access reactive centers is of importance. Our quenching studies coupled with the results of Schuh and associates,[48–50] Barboy and Feitelson,[30,31] Papp et al.,[45] and Brunet et al.,[63] indicate that the heme group in HRP is much more protected than the heme in myoglobin and metal-substituted hemoglobin. The remarkable finding is that the addition of the substrate analog drastically affects the penetration of oxygen, as indicated by the magnitude of the oxygen quenching rate constant. The quenching constant was reduced by a factor of 6 at 25°C.

The viscosity dependence of the quenching rate constants provides additional evidence that the diffusion of oxygen through the protein proceeds through a specific channel. The viscosity dependence for the oxygen quenching rate constant in proteins is expressed with a power law having an exponent (-0.7) in terms of the viscosity. This is much larger than the exponent (-0.4) observed for the oxygen quenching rate of the reference dendrimer (PdPorphGlu^{3}OH). Both exponents reflect the dependence of the diffusion constants D_S and D_P on solvent viscosity. The diffusion constant D_P demonstrates a larger viscosity dependence than D_S, as exhibited by their respective exponent values. The larger exponent seen in D_P may indicate that the passage of oxygen through the pore depends on protein motion; that is, protein in motion opens and closes the pore entrance, thereby controlling the oxygen access. In fact, the passage of oxygen might be a classic example of motion through a fluctuating entry point "bottleneck," as described by Zwanzig.[47] The exponent (-0.7) is quite consistent with the fluctuating bottleneck model.

The simulation results led us to hypothesize that the major access of oxygen to the heme site is through the region of the pore between Phe68 and Phe142, and that their conformations may determine the accessibility of oxygen to the interior. In the presence of BHA, the Phe68 phenyl ring blocks the pore region, reducing the area of the pore. The position of BHA in the X-ray structure 2ATJ and its small mobility in the simulations (the fluctuation of the distance between center of masses of BHA and of the heme is less than 1 Å) also suggest that this region serves as the entrance of oxygen. Considering the low accessibility of the heme to O_2 in the presence of BHA, the conformational fluctuations of Arg178 may not influence the penetration as significantly as those of Phe68 and Phe142. The results from the simulations also show that there are appreciable conformational dynamics of Phe68 and Phe142. Also, the protein dynamics are sensitive to the charges in the interior of the protein. In the absence of BHA, we observe that, for different charge states of the histidines, there are three different conformations of Phe68. At the charge state corresponding to low pH, Phe68 has an average conformation, very close to that in the X-ray structure. At high pH, Phe68 has a different structure from that of the X-ray structure, though the Leu does not block the entrance to the pore. Finally, at very high pH, the average conformation is even more drastically changed from that of the 1ATJ X-ray structure, resembling the X-ray structure 2ATJ when BHA is present.

We hence speculate that a wide range of conformations is accessed by Phe68, from open to closed pore states. Also, the population of these states, and the rate of fluctuations between them, may be altered by the charges on the protein and, hence, changes in pH. The residue Phe142 shows a less dramatic range of motion, but the two major

TABLE III. Average Dihedral Angles

Dihedral angle	1ATJ	2ATJ	Low pH	High pH	Very high pH (Leu)
phi 68	−56	−67	−62	−76	−54
psi 68	−40	118	−24	90	−38
chi1 68	−57	174	−60	64	−180
chi2 68	−45	55	−40	120	−113
phi 142	−90	−95	−100	−100	−105
psi 142	9	5	5	5	17
chi1 142	57	48	−60	−60	47
chi2 142	82	78	120	120	82
phi 178	−51	−50	−44	−51	−41
psi 178	−33	−32	−33	−25	−34
chi1 178	77	69	95	95	−160
chi2 178	67	79	180	160	180
chi3 178	67	79	180, 70	70	−60, 60
chi4 178	−105	−107	180	120	−90, −150

The averages of dihedral angles calculated from the MD trajectories 1, 3, 5, and 7 of HRP without BHA are compared with those from both crystal structures: 1ATJ (without BHA) and 2ATJ (with BHA). In cases of several transitions between two distinct conformers, the average value was computed separately for each conformer, and the major conformer is listed first, followed by the minor one (e.g., chi3 of Arg178 at low pH).

conformations observed in one case reduce the pore size and in the other increase it.

The extensive work in the realm of room temperature phosphorescence of proteins indicates that the quenching process is coupled to the long-range, low-frequency motions of the polypeptide backbone. The viscosity modulation of the quenching process also indicates that the dye dynamic change associated with the quenching process occurs in the macro-millisecond time scale. Our MD simulations are done in the pico-second time scale. We observe that both substrate and pH modulate the short-time frequency dynamics of the protein in the near vicinity of the heme pocket. The opening and closing of the channel is a low-frequency, large-amplitude motion. Our experimental results are in the long time scale, and our MD calculations have been performed in the short time scale. However, it seems that they are both influenced similarly by substrate and pH. This points to the fact that the long-range motion is diffusive in origin; that is, it is the outcome of a series of short-range motions of the protein residues, as seen in the simulation. Therefore, external stimuli that affect the short-range motions eventually lead to an observable effect in the long time scale.

The fluctuating entry point model[47] explains how the accessibility is affected by the substrate. The substrate not only blocks the bottleneck but it also makes the protein more rigid. This lowers the frequency at which the bottleneck fluctuates, causing the diffusion of molecules inside the protein to become more restricted. As strongly suggested by the structure of the pore region (Fig. 7) and supported by our quenching measurements, we conclude that small-molecule O_2, and by extrapolation, H_2O_2, diffuses through the pore.

Porphyrin represents a large target for the reaction with O_2. The binding of BHA occurs on the distal side, and X-ray analysis indicates little change in the overall protein conformation. If the protein matrix is assumed to behave like a homogeneous viscous medium, oxygen would be able to access each side of the porphyrin with equal probability. In this case, because BHA is much smaller than the porphyrin, one might expect that BHA would have no effect on the diffusion of oxygen leading to the proximal side and a small effect on diffusion through the protein leading to the distal side. The conformational change by BHA is mainly in the near vicinity of the channel, and BHA directly covers only a small portion of the porphyrin. Therefore, its direct effect would reduce the factor of 2 even more. However, BHA has a large effect on the diffusion of oxygen toward the heme. This is consistent with the view that oxygen accesses the heme via a channel that is close to the BHA binding site. When BHA binds to the protein, both the size and the motion of the residues making up the channel are affected, causing the large effect observed when the substrate binds the protein. The motion of small molecules through myoglobin also seems to occur via specific pathways, and the existence of specific cavities acting as docking sites has been experimentally verified.[64,65]

Diffusion-limited reactions through homogeneous solvents typically have low energies of activation. These values are normally between 3 and 6 kcal/mol for substances diffusing through water or organic solvents, depending on the temperature dependence of solvent viscosity and the validity of the Stokes–Einstein approximation.[66] The energy of activation for all the conditions for the protein system studied here are somewhat higher than

this (Table I), whereas the dendrimer results fall right within this bracket. In the case of proteins, O_2 is only slightly larger than the H_2O molecules that it must replace. Any reaction in a protein must involve concerted motions of many groups (in this case, fluctuation of the bottleneck), and it is therefore difficult to interpret energies of activation in terms of motions of particular atomic groups.

The sequence of the reactions of HRP with aromatic substrates is characterized as a ping-pong mechanism, meaning that the enzyme E1 first reacts with one substrate to form E2, which then reacts with the second substrate.[67] H_2O_2 binds much more easily when the aromatic substrate is not present. Therefore, the reaction between H_2O_2 and protein to form the ferryl intermediate occurs first. (The aromatic substrate can bind to the resting protein, but because it does not react with the protein, this does not change the enzymatic order.) The accomplishment of the ping-pong mechanism is aided by the rather simple fact that the second substrate prevents the first from accessing the heme, thereby preventing further reaction at the active site.

These results also answer an important question regarding the bioluminescent properties of HRP. It is well known that HRP can convert isobutanal into acetone, that is, in its excited triplet state.[68] The lifetime of the triplet state produced enzymatically is comparable to the lifetime of the triplet acetone produced by the thermal decomposition of dioxetane in deoxygenated media. This indicates that the excited triplet acetone remains inside the enzyme and is protected from ambient oxygen by the enzyme. The fact that oxygen can only penetrate the heme pocket through a specific pathway and the binding of substrate can limit the passage of oxygen toward the heme pocket may be the reason for the long lifetime observed for enzymatically produced excited triplet acetone.

CONCLUSIONS

We have elucidated the mechanism which molecular oxygen penetrates HRP. These molecules can access the heme pocket through a specific pathway. The diffusion of small molecules from the protein surface toward the heme pocket can be characterized by motion through a fluctuating bottleneck. It is this relative impermeability toward oxygen that leads to the unique bioluminescent properties of peroxidase proteins.

ACKNOWLEDGMENTS

We acknowledge informative discussions and a generous gift of BNS by Professor M.D. Schuh of Davidson College. Our thanks also to Wayne Wright, University of Pennsylvania, for technical support.

REFERENCES

1. Perutz MF. Regulation of oxygen affinity of hemoglobin: Influence of structure of the globin on the heme iron. Annu Rev Biochem 1979;48:327–386.
2. Ansari A, Di Iorio EE, Dlott DD, Frauenfelder H, Iben IET, Langer P, Roder H, Sauke TB, Shyamsunder E. Ligand binding to heme proteins: Relevance of low-temperature data. Biochemistry 1986; 25:3139–3146.
3. Austin RH, Beeson K, Eisenstein L, Faruenfelder H, Gunsalus IC, Marshall VP. Dynamics of carbon monoxide binding by heme proteins. Science 1973;181:541–543.
4. Beece D, Eisenstein L, Fraunfelder H, Good D, Marden MC, Reinisch L, Reynolds AH, Sorensen LB, Yue KT. Solvent viscosity and protein dynamics. Biochemistry 1980;19:5147–5157.
5. Doster W, Bowne SF, Frauenfelder H, Reinisch L, Shyamsunder E. Recombination of carbon monoxide to ferrous horseradish peroxidase types A and C. J Mol Biol 1987;194:299–312.
6. Frauenfelder H, Petsko GA, Tsernoglou D. Temperature-dependent X-ray diffraction as a probe of protein structural dynamics. Nature 1979;280:558–563.
7. Frauenfelder H, Sligar SG, Wolynes PG. The energy landscapes and motions of proteins. Science 1991;254:1598–1603.
8. Steinbach PJ, Ansari A, Berendzen J, Braunstein D, Chu K, Cowen BR, Ehrenstein D, Frauenfelder H, Johnson JB. Ligand binding to heme proteins: Connection between dynamics and function. Biochemistry 1991;30:3988–4001.
9. Hagen SJ, Hofrichter J, Eaton WA. Geminate rebinding and conformational dynamics of myoglobin embedded in a glass at room temperature. J Phys Chem 1996;100:12008–12021.
10. Hagen SJ, Hofrichter J, Eaton WA. Protein reaction kinetics in a room-temperature glass. Science 1995;269:959–962.
11. Ansari A, Jones CM, Henry ER, Hofrichter J, Eaton WA. The role of solvent viscosity in the dynamics of protein conformational changes. Science 1992;256:1796–1798.
12. Gottfried DS, Peterson ES, Sheikh AG, Wang J, Yang M, Friedman JM. Evidence for damped hemoglobin dynamics in a room temperature trehalose glass. J Phys Chem 1996;100:12034–12042.
13. Falconi IM, O'Neill P, Stroppolo ME, Desideri A. Superoxide dismutase kinetics. Methods Enzymol 2002;349:38–49.
14. Amara P, Andreoletti P, Jouve HM, Field MJ. Ligand diffusion in the catalase from *Proteus mirabilis:* A molecular dynamics study. Protein Sci 2001;10;1927–1935.
15. Gratton E, Jameson DM, Weber G, Alpert B. A model of dynamic quenching of fluorescence in globular proteins. Biophys J 1984;45: 789–794.
16. Lakowicz JR, Weber G. Quenching of fluorescence by oxygen: Probe for structural fluctuations in macromolecules. Biochemistry 1973;12:4161–4170.
17. Lakowicz JR, Weber G. Quenching of protein fluorescence by oxygen: Detection of structural fluctuations in proteins on the nanosecond time scale. Biochemistry 1973;12:4171–4179.
18. Vanderkooi JM. Tryptophan phosphorescence from proteins at room temperature. Topics Fluoresc Spectrosc 1992;3:113–136.
19. Subramaniam V, Steel DG, Gafni A. Room temperature tryptophan phosphorescence as a probe of structural and dynamic properties of proteins. Topics Fluoresc Spectrosc 2000;6:43–65.
20. Calhoun DB, Englander SW, Wright WW, Vanderkooi JM. Quenching of room temperature protein phosphorescence by added small molecules. Biochemistry 1988;27:8466–8474.
21. Cioni P, Strambini GB. Acrylamide quenching of protein phosphorescence as a monitor of structural fluctuations in the globular fold. J Am Chem Soc 1998;120:11749—11757.
22. Strambini GB, Cioni P. Pressure–temperature effects on oxygen quenching of protein phosphorescence. J Am Chem Soc 1999;121: 8337–8344.
23. Fischer CJ, Schauerte JA, Wisser KC, Gafni A, Steel DG. Hydrogen exchange at the core of *Escherichia coli* alkaline phosphatase studied by room-temperature tryptophan phosphorescence. Biochemistry 2000;39:1455–1461.
24. Fischer CJ, Schauerte JA, Wisser KC, Steel DG, Gafni A. Differences in the pathways for unfolding and hydrogen exchange among mutants of *Escherchia coli* alkaline phosphatase. Biochim Biophys Acta 2001;1545:96–103.
25. Schlyer BD, Steel DG, Gafni A. Long time-scale probing of the protein globular core using hydrogen-exchange and room temperature phosphorescence. Biochem Biophys Res Commun 1996;223: 670–674.
26. Somogyi B, Norman JA, Rosenberg A. Gated quenching of intrinsic fluorescence and phosphorescence of globular proteins: An extended model. Biophys J 1986;50:55–61.
27. Sonmogyi B, Norman JA, Punyiczki M, Rosenberg A. Viscosity dependence of acrylamide quenching of ribonuclease T1 fluorescence: The gating mechanism. Biochim Biophys Acta 1992;1119: 81–98.

28. Somogyi B, Lakos Z. Protein dynamics and fluorescence quenching. J Photochem Photobiol B 1993;18:3–16.
29. Eftink MR, Hagaman KA. Fluorescence quenching of the buried tryptophan residue of cod parvalbumin. Biophys Chem 1985;22: 173–180.
30. Barboy N, Feitelson J. Quenching of the zinc-protoporphyrin triplet state as a measure of small-molecule diffusion through the structure of myoglobin. Biochemistry 1987;26:3240–3244.
31. Barboy N, Feitelson J. Diffusion of small molecules through the structure of myoglobin: Environmental effects. Biochemistry 1989; 28:5450–5456.
32. Chance B. Catalase and peroxides: II. The kinetics and stoichiometry of the transition from primary to the secondary peroxidase peroxide complexes. Arch Biochem Biophys 1952;41;416–424.
33. Danner DJ, Brignac PJ Jr, Arceneaux D, Patel V. Oxidation of phenol and its reaction product by horseradish peroxidase and hydrogen peroxide. Arch Biochem Biophys 1973;156:759–763.
34. Porter DJT, Bright HJ. The mechanism of oxidation of nitroalkanes by horseradish peroxidase. J Biol Chem 1983;258:9913–9924.
35. Aviram I. The interaction of benzhydroxamic acid with horseradish peroxidase and its fluorescent analogs. Arch Biochem Biophys 1981;212:483–490.
36. Aitken SM, Turnbull JL, Percival MD, English AM. Thermodynamic analysis of the binding of aromatic hydroxamic acid analogues to ferric horseradish peroxidase. Biochemistry 2001;40: 13980–13989.
37. Fidy J, Paul KG, Vanderkooi JM. Differences in the binding of aromatic substrates to horseradish peroxidase revealed by fluorescence line narrowing. Biochemistry 1989;28:7531–7541.
38. Horie T, Vanderkooi JM, Paul KG. Study of the active site of horseradish peroxidase isoenzymes A and C by luminescence. Biochemistry 1985;24:7934–7941.
39. Henriksen A, Schuller DJ, Meno K, Welinder KG, Smith AT, Gajhede M. Structural interactions between horseradish peroxidase C and the substrate benzhydroxamic acid determined by X-ray crystallography. Biochemistry 1998;37:8054–8060.
40. Indiani C, Feis A, Howes BD, Marzocchi MP, Smulevich G. Benzohydroxamic acid-peroxidase complexes: Spectroscopic characterization of a novel heme spin species. J Am Chem Soc 2000;122:7368–7376.
41. Rich PR, Wiegand NK, Blum H, Moore AL, Bonner WD Jr. Studies on the mechanism of inhibition of redox enzymes by substituted hydroxamic acids. Biochim Biophys Acta 1978;525:325–337.
42. Veitch NC, Williams RJP. The use of methyl-substituted benzhydroxamic acids as structural probes of peroxidase substrate binding. Eur J Biochem 1995;229:629–640.
43. Callis JB, Gouterman M, Jones YM, Henderson BH. Porphyrins: XXII. Fast fluorescence, delayed fluorescence, and quasiline structure in palladium and platinum complexes. J Mol Spectrosc 1971;39:410–420.
44. Eastwood D, Gouterman M. Porphyrins. XVIII: Luminescence of cobalt, nickel, palladium, platinum complexes. J Mol Spectrosc 1970;35:359–375.
45. Papp S, Vanderkooi JM, Owen CS, Holtom GR, Phillips CM. Reactions of excited triplet states of metal substituted myoglobin with dioxygen and quinone. Biophys J 1990;58:177–186.
46. Vinogradov SA, Lo L-W, Wilson DF. Dendritic polyglutamic porphyrins: Probing porphyrin protection by oxygen-dependent quenching of phosphorescence. Chem Eur J 1999;5:1338–1347.
47. Zwanzig R. Dynamical disorder: Passage through a fluctuating bottleneck. J Chem Phys 1992;97:3587–3589.
48. Bayles SW, Beckham S, Leidig PR, Montrem A, Taylor ML, Wright TM, Wu Y, Schuh MD. Demonstration that phosphorescent 6-bromo-2-naphthyl sulfate can be used to probe heme accessibility in heme proteins. Photochem Photobiol 1991;54:175–181.
49. Beckham S, Cook MP, Karki L, Luchsinger MM, Whitlock VR, Wu Y, Zhang Q, Schuh MD. Heme protein dynamics studied by phosphorescence of an external phosphorescent probe molecule. Arch Biochem Biophys 1994;310:440–447.
50. Coates AI, Cook MP, Feezor R, Schuh MD. Dependence of heme accessibility in horseradish peroxidase on Ca^{2+}. J Inorg Biochem 1998;72:63–69.
51. Kaposi AD, Fidy J, Manas ES, Vanderkooi JM, Wright WW. Horseradish peroxidase monitored by infrared spectroscopy: Effect of temperature, substrate and calcium. Biochim Biophys Acta 1999;1435:41–50.
52. Paul KG. Isolation of horseradish peroxidase. Acta Chem Scand 1958;12:1312–1318.
53. Vanderkooi JM, Moy VT, Maniara G, Koloczek H, Paul KG. Site-selected fluorescence spectra of porphyrin derivatives of heme proteins. Biochemistry 1985;24:7931–7935.
54. Rozhkov V, Wilson D, Vinogradov S. Phosphorescent Pd porphyrin-dendrimers: Tuning core accessibility by varying the hydrophobicity of the dendritic matrix. Macromolecules 2002;35:1991–1993.
55. Vinogradov SA, Fernandez-Searra MA, Dugan BW, Wilson DF. Frequency domain instrument for measuring phosphorescence lifetime distributions in heterogeneous samples. Rev Sci Instrum 2001;72:3396–3406.
56. MacKerell AD Jr, Bashford D, Bellott M, Dunbrack RL, Evanseck JD, Field MJ, Fischer S, Gao J, Guo H, Ha S, Joseph-McCarthy D, Kuchnir L, Kuczera K, Lau FTK, Mattos C, Michnick S, Ngo T, Nguyen DT, Prodhom B, Reiher WE III, Roux B, Schlenkrich M, Smith JC, Stote R, Straub J, Watanabe M, Wiorkiewicz-Kuczera J, Yin D, Karplus M. All-atom empirical potential for molecular modeling and dynamics studies of proteins. J Phys Chem B 1998:3586–3616.
57. Brooks BR, Bruccoleri RE, Olafson BD, States DJ, Swaminathan S, Karplus M. CHARMM: A program for macromolecular energy, minimization, and dynamics calculations. J Comput Chem 1983;4: 187–217.
58. Grant JA, Pickup BT, Nicholls A. A smooth permittivity function for Poisson–Boltzmann solvation methods. J Comput Chem 2001; 22:608–640.
59. Gajhede M, Schuller DJ, Henriksen A, Smith AT, Poulos TL. Crystal structure of horseradish peroxidase C at 2.15 Å resolution. Nat Struct Biol 1997;4:1032–1038.
60. Jordan J, Bauer WE. Correlations between solvent structure, viscosity, and polarographic diffusion coefficients of oxygen. J Am Chem Soc 1959;81:3915–3919.
61. CRC. Handbook of chemistry and physics. Cleveland: Chemical Rubber Publishing Co.; 1958.
62. Khajehoour M, Vanderkooi JM, Troxler T. The effect of protein dynamics upon reactions that occur in the heme-pocket of horseradish peroxidase. Biochemistry 2003, 42, 2672.
63. Brunet JE, Jullian C, Jameson DM. Oxygen diffusion through horseradish peroxidase. Photochem Photobiol 1990;51:487–489.
64. Brunori M. Structural dynamics of myoglobin. Biophys Chem 2000;86:221–230.
65. Brunori m, Gibson QH. Cavities and packing defects in the structural dynamics of myoglobin. EMBO Rep 2001;2:674–679.
66. Steinfeld JI, Francisco JS, Hase WL. Chemical kinetics dynamics. 2nd edition. Upper Saddle River, NJ: Prentice-Hall; 1999. 544 p.
67. Kedderis GL, Hollenberg PF. Characterization of the *N*-demethylation reactions catalyzed by horseradish peroxidase. J Biol Chem 1983;258:8129–8138.
68. Faria Oliveria OMM, Haun M, Duran N, O'Brien PJ, O'Brien CR, Bechara EJH, Cilento G. Enzyme-generated electronically excited carbonyl compounds: Acetone phosphorescence during the peroxidase-catalyzed aerobic oxidation of isobutanal. J Biol Chem 1978;253:4707–4712.